ADVANCED SUSTAINABLE SYSTEMS
www.advsustainsys.com



# Sustainable Cathodes for Lithium-Ion Energy Storage Devices Based on Tannic Acid—Toward Ecofriendly Energy Storage

*Ivan K. Ilic,* Alexandra Tsouka, Milena Perovic, Jinyeon Hwang, Tobias Heil, Felix F. Loeffler, Martin Oschatz, Markus Antonietti, and Clemens Liedel**

**The use of organic materials with reversible redox activity holds enormous potential for next-generation Li-ion energy storage devices. Yet, most candidates are not truly sustainable, i.e., not derived from renewable feedstock or made in benign reactions. Here an attempt is reported to resolve this issue by synthesizing an organic cathode material from tannic acid and microporous carbon derived from biomass. All constituents, including the redox-active material and conductive carbon additive, are made from renewable resources. Using a simple, sustainable fabrication method, a hybrid material is formed. The low cost and ecofriendly material shows outstanding performance with a capacity of 108 mAh $g^{-1}$ at 0.1 A $g^{-1}$ and low capacity fading, retaining approximately 80% of the maximum capacity after 90 cycles. With approximately 3.4 V versus $Li^+$/Li, the cells also feature one of the highest reversible redox potentials reported for biomolecular cathodes. Finally, the quinone-catecholate redox mechanism responsible for the high capacity of tannic acid is confirmed by electrochemical characterization of a model compound similar to tannic acid but without catecholic groups.**

## 1. Introduction

Lithium-ion batteries are the most prominent energy storage devices in applications that require high energy densities (e.g., in smartphones or electrical vehicles). Unfortunately, these established energy storage devices are still rather unsustainable, expensive, prone to fire, or explosion upon malfunction.[1,2] The most common cathode materials in conventional energy storage devices are inorganic materials such as $LiCoO_2$, $LiFePO_4$, or $LiMn_2O_4$ and are often based on unsustainable and toxic heavy metals.[3,4] In terms of sustainability and price, especially energy storage devices based on organic electrodes, which utilize redox-active organic materials, are considered promising candidates for next-generation batteries.[5–7] Unlike conventional inorganic electrodes, which generally operate by an intercalation mechanism during charging and discharging, organic energy storage devices feature storage-release reactions of $Li^+$ at distinct organic redox-active sites near surfaces. This enables higher rate capability and longer cycle life as there are no lattice transformations, transport limitations, and heat generation, which usually deteriorates the lifetime of inorganic cathode materials. Moreover, organic energy storage devices can be excellent candidates for flexible and stretchable devices in wearable electronics.[8,9]

Many redox-active and lithium coordinating organic molecules such as anthraquinones, imides, flavins, organosulfur compounds, radicals, and their derivatives have been investigated as cathode materials in the past.[10] Establishment of batteries with long lifetime and high specific energy requires a large redox potential versus Li/$Li^+$, redox reactions involving multiple electrons, and high stability against electrochemical degradation.

Quinones, and related structures that can be oxidized to quinones such as guaiacyl and catecholic groups, are promising redox-active subunits for the formation of energy storage devices.[11] Additionally, these organic functionalities are widespread in organic polymers such as lignin[12,13] and tannic acid. The redox reactivity of lignin, a guaiacyl rich polymer, was studied in detail in aqueous electrolyte, confirming the initial oxidation to quinones and subsequent reversible redox transformation of quinones to hydroquinones.[14] Later, redox reactivity of catecholic groups was confirmed in lithium-organic electrolytes, suggesting the equivalent redox couple.[15] Similar mechanism was suggested for tannic acid, ester of glucose and multiple gallic acids,[16] that is rich with catecholic groups.[17,18] The good solubility of tannic acid in water and polar organic solvents of low toxicity, such as ethanol, allows for the easy

I. K. Ilic, M. Perovic, J. Hwang, Dr. T. Heil, Dr. M. Oschatz, Prof. M. Antonietti, Dr. C. Liedel
Department of Colloid Chemistry
Max Planck Institute of Colloids and Interfaces
Am Mühlenberg 1, Potsdam 14476, Germany
E-mail: ivan.ilic@mpikg.mpg.de; clemens.liedel@mpikg.mpg.de

A. Tsouka, Dr. F. F. Loeffler
Department of Biomolecular Systems
Max Planck Institute of Colloids and Interfaces
Am Mühlenberg 1, Potsdam 14476, Germany

A. Tsouka
Department of Chemistry and Biochemistry
Freie Universität Berlin
Arnimalle 22, Berlin 14195, Germany

Dr. M. Oschatz
Institute of Chemistry
University of Potsdam
Karl-Liebknecht-Straße 24–25, Potsdam 14476, Germany

The ORCID identification number(s) for the author(s) of this article can be found under https://doi.org/10.1002/adsu.202000206.



**DOI: 10.1002/adsu.202000206**

extraction from plant-based waste such as wood bark.[19] On the other side, tannic acid is also well soluble in the solvents typically applied as electrolytes, seriously limiting its applicability in electrochemical devices.

One approach to reducing the apparent solubility of tannic acid and increase conductivity utilizes graphene sheets to stabilize tannic acid by $\pi$–$\pi$ interactions. Here, tannic acid additionally acts as a binder in the formed composite, and no halogenated binders are needed.[20] However, graphene as such is a rather sophisticated material for the use in battery electrodes at scale and, therefore, not suitable for truly sustainable electrodes.

To increase conductivity and prevent dissolution, tannic acid may also be immobilized in a crosslinked polypyrrole network.[18] Additionally, crosslinking using heavy metal ions was also reported as an efficient way to prevent dissolution.[17,21] Adding polypyrrole or other conductive polymers, however, decreases the sustainability of the electrode production as the building blocks for such polymers are usually obtained by petrochemical processes. High surface area carbon additives obtained from renewable sources are surely more benign. In these additives, the surface area of the carbon material significantly affects the electrode performance. Large surface areas can contribute to the stable fixation of redox-active organic materials onto the carbon and maximize the exposed reaction sites located at the interface to the electrolyte.[22]

The synthesis of hybrid organic charge storage material as performed in this study requires a combined approach. In the first step, ball milling of tannic acid (TAN), the redox-active organic material, together with carbon black as a conductive additive, creates a composite with strong interaction between the individual compounds. Propylene glycol is used as a sustainable and nontoxic solvent to prepare a slurry of the composite. The final electrodes have TAN firmly bound onto the carbon black, and the whole fabrication process is conducted with ecofriendly chemicals forming truly sustainable electrodes.

We use the so prepared electrodes as cathodes for sustainable organic energy storage devices, without any nonsustainable binder or auxiliary supporting materials. Through material characterizations and various electrochemical analyses, it is confirmed that the tannic acid-based material can be utilized in traditional lithium electrochemical energy storage systems. This study is an attempt to fabricate exceptionally ecofriendly cathode materials, which will help to establish sustainable, flexible, disposable, and nonexplosive organic energy storage devices in the future.

## 2. Results and Discussion

### 2.1. Synthesis and Characterization of C/TAN

For immobilization and improvement of conductivity of tannic acid, a hybrid material with sustainable, sucrose-derived, porous carbon (C(pristine)) was prepared. The synthesized carbon primarily shows the behavior of a microporous system with a significant contribution to the total pore volume by narrow mesopores (Figure S1 and Table S2, Supporting Information). This allows for the tannic acid to penetrate the structure, forming a stable composite.

Ball milling was used to prepare a hybrid material between TAN and C(pristine) (**Figure 1**). Several combinations of neat grinding and liquid assisted-grinding were investigated (**Table 1**). Stainless steel jars equipped with stainless steel balls were used for the preparation of hybrid materials, resulting in contamination of the materials by iron as examined with ICP-OES (**Figure 2**a). As expected, C(pristine) contains almost no iron. However, during neat grinding it gets contaminated with approximately 10 wt% iron, as can be observed from ICP-OES of C(50 min) and C(50 min)/TAN, whereas the iron content is somewhat smaller in the latter case due to the late addition of tannic acid. Iron contamination is reduced significantly if TAN is added immediately together with carbon, as can be seen for C/TAN. This can be even further reduced by omitting neat grinding as shown for C/TAN(PG). These results suggest that the ball milling induces additional defects into the porous carbon network, which then react with iron from the steel jar. However, the results also suggest that upon addition of tannic acid and/or solvent, carbon rather reacts with the organic constituents of the blend. These conclusions are confirmed by

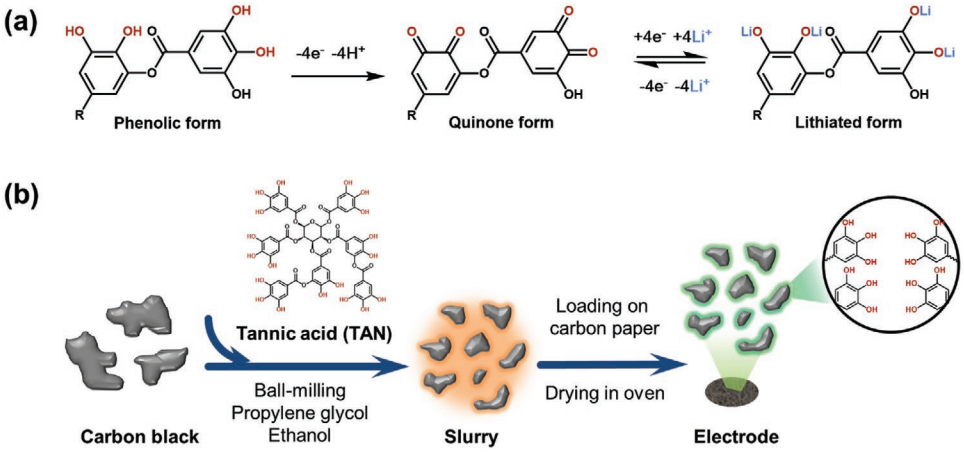


**Figure 1.** a) Tannic acid has a high density of redox-active *o*-hydroquinones. b) To assure good contact between tannic acid and microporous carbon, the two were ball milled, facilitating the formation of $\pi$–$\pi$ stacking between the microporous carbon and tannic acid.

**Table 1.** Different ball milling procedures of C(pristine) and TAN.

| Name | C(pristine) [mg] | TAN [mg] | Grinding method |
|---|---|---|---|
| C(50 min) | 54 | 0 | Neat ground for 50 min |
| C(50 min)/TAN | 36 | 24 | C(pristine) was neat ground for 50 min, and afterwards, TAN in PG was added for an additional 10 min |
| C/TAN | 36 | 24 | C(pristine) and TAN were neat ground for 50 min, and afterwards, PG was added for an additional 10 min |
| C/TAN(PG) | 36 | 24 | C(pristine) and TAN were mixed with PG and ground for 60 min |

elemental analysis (Table S1, Supporting Information). A significant drop in the carbon content of C(50 min) compared to C(pristine) as well as a rapid increase in oxygen content suggest a reaction of the carbon with the environment (Table S1, Supporting Information). Similar reactions of carbons with the surrounding media in the ball mill have been described previously.[23–26]

Crosslinking of TAN with iron salts is the most studied method of tannic acid immobilization for electrochemical energy storage,[17,21] and therefore the influence of iron content on tannic acid leakage had to be further investigated. We employed UV-Vis spectroscopy for this purpose. For these measurements, the hybrid materials C(50 min)/TAN, C/TAN, and C/TAN(PG) were ultrasonicated with ethanol, and afterwards, the carbon was removed by filtration. By calibration with samples containing a known concentration of tannic acid (Figure S2, Supporting Information), the amount of leaked tannic acid, compared to the theoretical amount of tannic acid in the composite, could be determined (Figure 2b). The amount of leaked tannic acid does not correlate with the iron content in the samples, leading to the conclusion that iron does not act as a crosslinking agent for tannic acid in our samples. Therefore, we conclude that certain chemical or physical binding between carbon and tannic acid is established in a ball mill, probably a combination of $\pi$–$\pi$ and electrostatic interactions,[27] forming a rather stable composite. It is important to mention that ultrasonication, a rather harsh method, results in the dissolution of more molecules than it would be the case during battery cycling.

Powder X-ray diffraction (PXRD) measurements were performed to further study the hybrid material (Figure 2c). C(pristine) shows multiple sharp diffraction lines, indicating a contamination with species of high crystallinity. This contamination could be ascribed to zinc sulfide,[28] most likely formed during the synthesis of the carbon material from leftover zinc species and sulfuric acid upon reduction (Figure S3, Supporting Information). However, the amount of zinc sulfide in C(pristine) is very low, as ICP measurements show only 8.87 (std. dev. 0.168) mg of zinc per gram of C(pristine), and this most likely does not influence electrochemical behavior as investigated below. The sharpness of diffraction lines, contrary to the abundance, can be ascribed to high crystallinity of the contamination in an amorphous matrix. Furthermore, zinc sulfide is not visible in C(50 min), probably as highly reactive

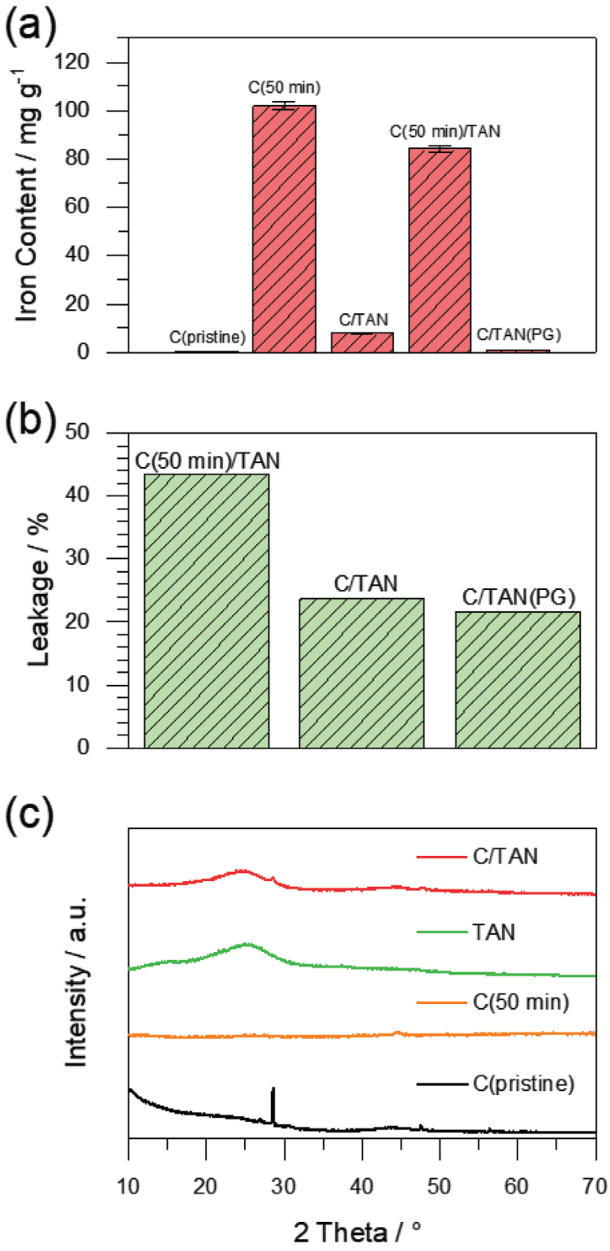


**Figure 2.** a) Iron content of C(pristine), C(50 min), and different composites of C and TAN prepared in a ball mill. b) Leakage of tannic acid from different C and TAN composites as determined from UV/Vis. c) PXRD of C(pristine), C(50 min), TAN, and C/TAN.

carbon disrupts the crystal structure, and broad peaks are visible in C/TAN. The latter can be explained as ball milling reduces the size of inorganic crystallites and increases the lattice-microstrain, ultimately causing a broadening of diffraction lines in powder XRD.[29] A characteristic broad diffraction line in the range of 25° is visible both in the diffractogram of TAN and C/TAN, suggesting the perseverance of $\pi$-$\pi$ stacking of tannic acid molecules and carbon in the composite.

The morphologies of different hybrid materials were compared using SEM (Figure S4, Supporting Information). All hybrid materials consist of aggregates of smaller particles.

Their size remains the same throughout all of the samples. However, the density of their packing is higher for C/TAN(PG) and C(50 min)/TAN compared to C/TAN.

STEM images of C/TAN were acquired to investigate the composite in more detail (**Figure 3**a). The sample mainly exhibits amorphous sheet structures with visible near-range order (Figure 3b). EDX mapping was performed to determine the chemical composition, mainly showing carbon and oxygen, but also iron and chromium, from stainless steel, zinc, and sulfur, from zinc sulfide, (Figure 3c), and also traces of calcium, sodium, and silicon, from glassware. Carbon, oxygen, iron, and chromium can be found in the same areas confirming the homogeneity of carbon-tannic acid composites at nano-level with minor iron and chromium impurities not organized into big particles, but rather being scattered through the sample, explaining why no iron or chromium compounds are seen in PXRD. In contrast, zinc and sulfur can be found concentrated in the same position, confirming the formation of grains of zinc sulfide as determined in PXRD rather than scattered throughout the sample. Due to the low amount of iron, EELS measurements did not provide a clear answer on the state of iron. However, EELS spectra of C(50 min) show the typical two-peak structure of the L-edge of iron (Figure S5, Supporting Information), with the first peak setting in at around 703 eV, suggesting the presence of iron in the oxidation states of 0 and II. However, due to the presence of a high amount of phenol groups in C/TAN iron may be present in higher oxidation states in these samples.

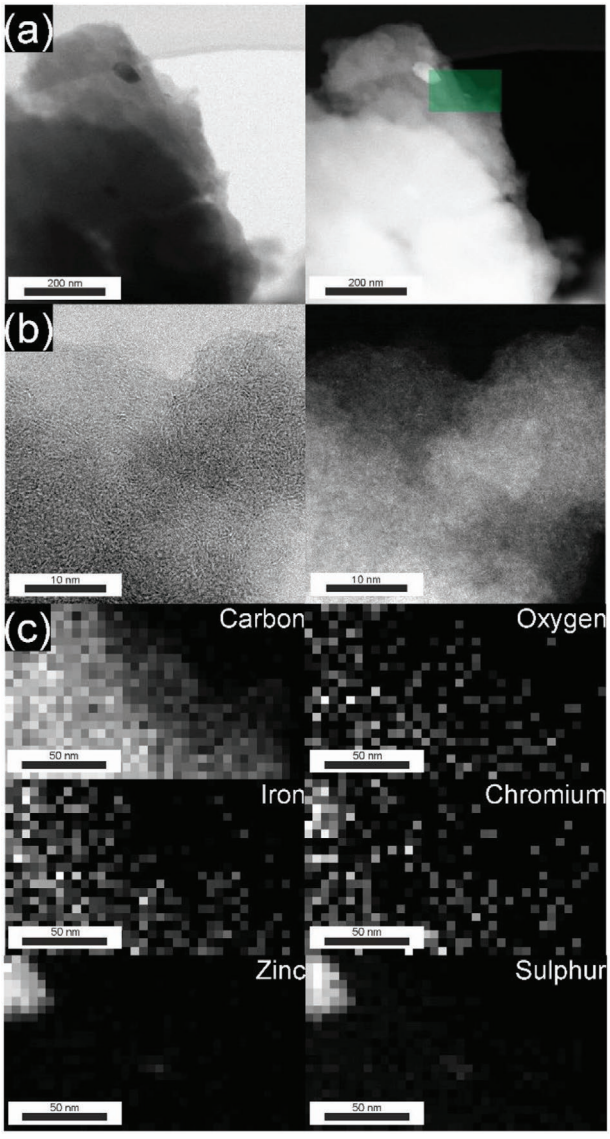


**Figure 3.** STEM images of C/TAN. a,b) Brightfield (left) and darkfield (right) images at different magnifications. c) EDX imaging mapping for the six strongest signals of the same region marked in (a).

### 2.2. Electrochemical Behavior of C/TAN

Finally, different composites of tannic acid were compared electrochemically (**Figure 4**). By far C(50 min)/TAN performs the worst which can be explained by bad contact between the carbon and the tannic acid as well as damaged structure of carbon upon 50 min of neat grinding. The best performance can be observed for C/TAN, while C/TAN(PG) performs similarly, but with a much bigger deviation between different samples and significantly lower stability.

The high reproducibility of C/TAN samples could be ascribed to a more homogenous electrode material formed upon neat ball milling of the carbon and the tannic acid, as the samples do not differ significantly in composition as determined by elemental analysis (Table S1, Supporting Information) and tannic acid leakage test (Figure 2b) along with the low iron-contamination of both samples (Figure 2a). The neat grinding of carbon and tannic acid and subsequent addition of the solvent was used as the method of choice for the preparation of cathodes in further electrochemical experiments as it exhibited optimal performance.

Concerning the electrochemical behavior of the material, conductivity, and permeability of the formed C/TAN were first investigated using EIS (Figure S6, Supporting Information). After plotting the results as Nyquist plot, the characteristic

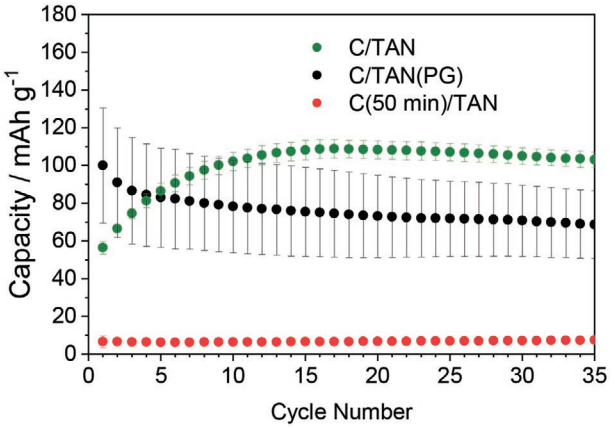


**Figure 4.** Electrochemical performance of C/TAN, C/TAN(PG), and C(50 min)/TAN during the charging–discharging test at 0.1 A $g^{-1}$.

shape of a semicircle followed by a straight line confirms good contact of all compounds and permeability to the electrolyte. The electrochemical performance of C/TAN was investigated using charging–discharging tests and cyclic voltammetry (**Figure 5**). During long term cycling at 0.1 A $g^{-1}$, the capacity raises during the first 17 cycles and slowly decreases afterward (Figure 5a). The early increase can be ascribed to the initial oxidation of TAN as well as the reorganization of the polymer during cycling, which leads to a better performing composite of TAN and C. The subsequently decreasing capacity can be primarily ascribed to the deactivation of redox-active groups and leakage of tannic acid.[18] However, the decrease in the capacity is rather low, with a capacity retention of 81.1% after 90 cycles.

Rate performance was determined by charging–discharging tests at varying current density, starting at 0.05 A $g^{-1}$ for 20 cycles, followed by 10 cycles each at 0.1, 0.2, 0.4, 0.8, 1.6, and 3.2 A $g^{-1}$, ultimately ending with 10 cycles at 0.05 A $g^{-1}$ (Figure 5b). As expected, the initial capacity rises within 12 cycles to 112.3 mAh $g^{-1}$, which slowly decreases again during the following cycles as observed before. While logically, the further decrease is observed every time the current density is doubled, a comparably high capacity of 45 mAh $g^{-1}$ is retained at a high current density of 3.2 A $g^{-1}$. Upon the reduction of the current density again to 0.05 A $g^{-1}$, a capacity of around 95 mAh $g^{-1}$ is regained, which is comparable to the capacity of the 20th cycle, the last one of initial cycling at the same current density. Therefore, we conclude that C/TAN can withstand current densities between 0.05 and 3.2 A $g^{-1}$ without significant degradation.

Charging–discharging curves of C/TAN lack the characteristic plateau expected for redox-active molecules (Figure 5c). In contrast, cyclic voltammetry of C/TAN (Figure 5d) clearly shows oxidation and reduction peaks. Similar behavior was previously observed for different hybrid materials containing tannic acid.[17,18] Reducing the cycling rates shifts the position of the peaks toward lower (higher) voltages for oxidation (reduction), indicating a semireversible behavior. The average redox potential is 3.4 V (vs $Li/Li^+$), which is relatively high compared to conventional organic materials[10] and outstanding when compared to other electrodes from waste biomass,[30] although similar to other cathodes utilizing catecholic groups (Table S3, Supporting Information).[15,31,32]

Furthermore, Faradaic, redox from tannic acid, and non-Faradaic, electric double layer from carbon, contributions to capacity were evaluated by separating current density in cycling voltammetry in a part that is linear with the scan rate and one that is linear with the square root of the scan rate.[15] This model stands except in the region of high and low voltages as can be seen from the $R^2$ value and easily explained by the abruptly changing currents at the limits of the measurement range (Figure S7c, Supporting Information). By integrating the non-Faradaic voltammogram and dividing it by the integrated area of the overall voltammogram, the non-Faradaic contribution (Figure S7b, Supporting Information) and subsequently the Faradaic contribution is determined. As expected, Faradaic contribution to capacity is maximized at the potentials where oxidation and reduction peaks are found (Figure S7a, Supporting Information). Overall, the Faradaic contribution to capacity is rather high, between 23.5% (at 25 mV $s^{-1}$) and 42.8% (at 5 mV $s^{-1}$).

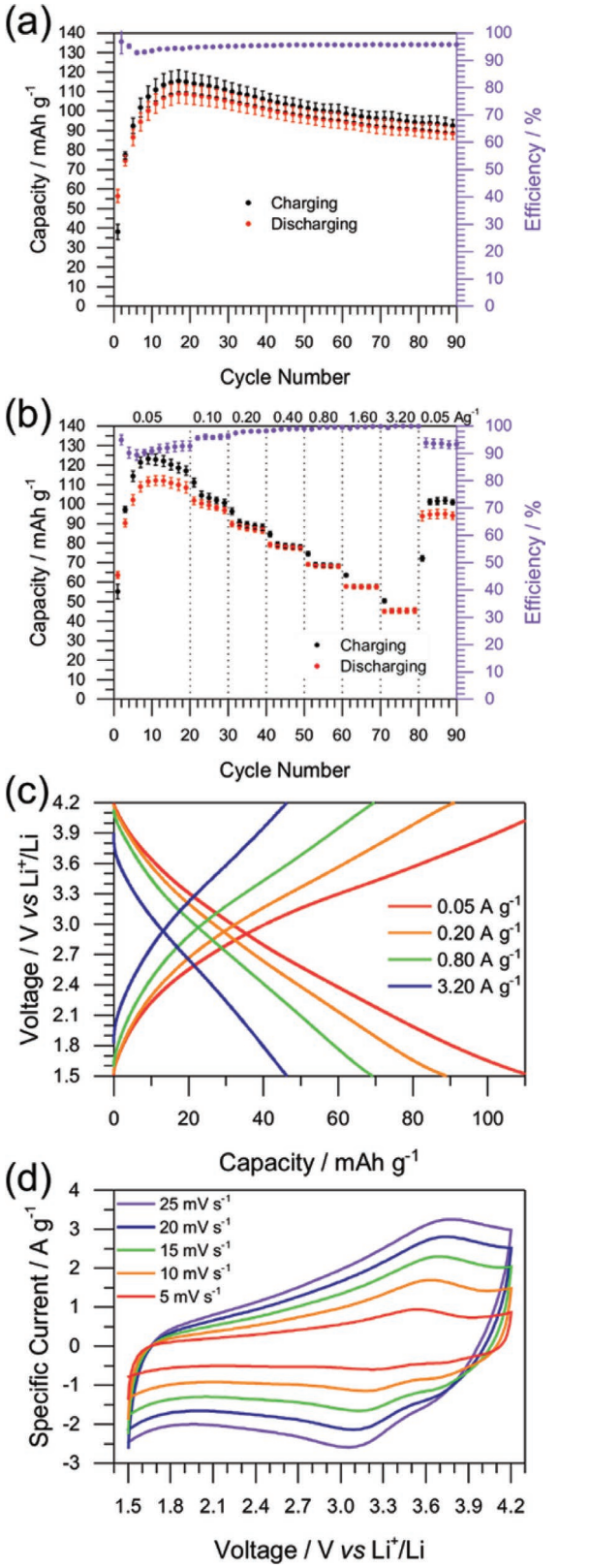


**Figure 5.** Electrochemical performance of C/TAN. a) Charging–discharging test at 0.1 A $g^{-1}$. b) Charging–discharging test at various current densities. c) Charging–discharging curves at selected current densities. d) Cyclic voltammetry at various scan rates.

### 2.3. Electrochemical Behavior of C/MOD

To confirm the suggested redox mechanism (Figure 1a), which assumes a quinone-catecholate redox pair, a model compound (MOD) was synthesized. The model compound has a structure similar to tannic acid (Scheme S1, Supporting Information) but it contains no phenolic groups in *ortho*-position, but rather only in *metha*, making them redox inactive as resorcinolic functionalities cannot get oxidized to the corresponding quinone. Additionally, hybrid material between sustainable carbon and MOD, C/MOD, cannot store electrons in any other way than by electric double layer formed on the surface of highly porous carbon. Therefore, the capacity of C/MOD is equivalent to the carbon, non-Faradaic, contribution to the capacity of C/TAN allowing as to asset contribution of the redox and electric double layer contributions to C/TAN experimentally, in addition to calculation. The capacity of carbon is often directly compared to the hybrid material containing carbon and redox-active polymer, a misguided practice, as we found out in our recent study.[15]

Consequently, as expected, cyclic voltammetry of C/MOD does not show the characteristic redox peaks of C/TAN (**Figure 6**a), pointing to the redox inactivity of C/MOD and confirming redox mechanism of tannic acid as suggested in Figure 1a. Furthermore, the Faradaic contribution to the capacity of C/TAN can be calculated by comparing the integration area of cyclic voltammograms of C/MOD and C/TAN. Depending on the scan rate, it results between 25% and 30% (Figure 6b), confirming numbers calculated from the scan-rate dependency of the current density. Finally, also the behavior of C/MOD at varying current densities (Figure 6c) further confirms the importance of redox-active groups in C/TAN hybrid material for charge storage properties.

## 3. Conclusion

Using tannic acid as an abundant, bioderived starting material and an ecofriendly ball milling process, sustainable cathode materials for organic lithium-based energy storage devices were prepared. Sucrose derived porous conductive carbon was used as a conductive additive, which, upon ball milling, forms stable hybrid material with tannic acid. Multiple ball milling methods were compared to find the optimal preparation procedure and the difference between the formed samples was discussed highlighting the need for in-depth investigation of composite electrode preparation. The formed material benefits from both battery like behavior, due to redox-active tannic acid, and supercapacitor-like behavior, due to the high surface area of the conductive carbon. The resulting structures and electrochemical behavior were extensively characterized, and the hybrid electrodes showed discharge capacities of 112.3 mAh $g^{-1}$ at 0.05 A $g^{-1}$ (1.0 M $LiPF_6$ in EC/DEC as electrolyte). The redox potential of 3.4 V, as determined by CV analysis, was shown to be very high for bioderived electrode materials. By comparing the performance of the C/TAN composite to a redox inactive model compound, the importance of redox moieties for the energy storage properties of C/TAN was highlighted and the proposed quinone–catecholate redox couple was confirmed. Furthermore, no oil-derived binder or carbon additives were

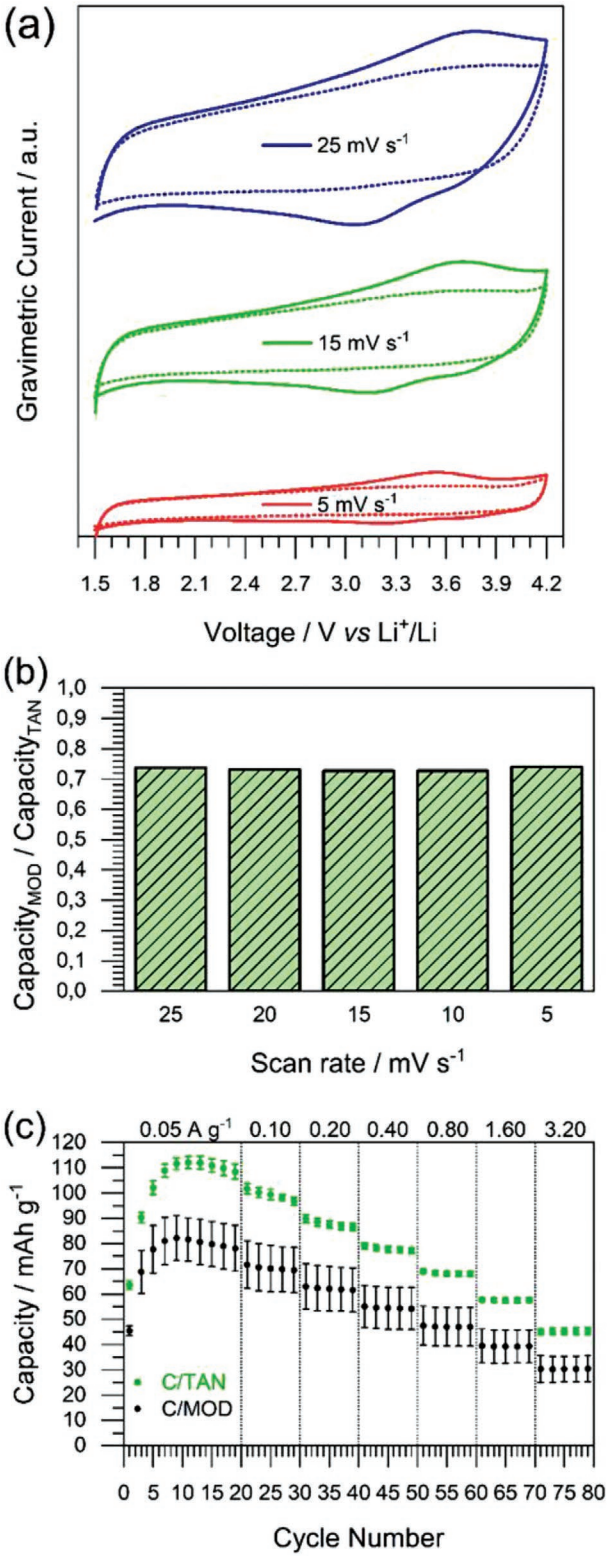


**Figure 6.** Comparison of electrochemical performance of C/TAN and C/MOD. a) Cyclic voltammetry at selected scan rates, full lines represent C/TAN, while dotted lines represent C/MOD. b) The ratio of capacities of C/MOD and C/TAN as calculated from cyclic voltammetry. c) Discharging capacities of C/TAN and C/MOD at varying current densities. Only every second point is shown for clarity.

necessary for the presented charge storage material, demonstrating the truly sustainable nature of the presented electrodes.

## 4. Experimental Section

*Materials*: Hydrolysable tannic acid (molecular weight of 1701.23 g $mol^{-1}$ as indicated by the supplier, Acros Organics, 95%) was used as received. Solvents ethanol (Fisher, >99%) and propylene glycol (Acros Organics, >99%) were used without purification.

*Synthesis of Sustainable Carbon*: $ZnCl_2$ was employed as the salt template for the synthesis of sustainable carbon.[33] 5 g of sucrose was dissolved in 15 mL of water, and 40 g of $ZnCl_2$ was dissolved in another 15 mL of water. The prepared solutions were mixed, and 0.55 g concentrated sulfuric acid was added. The mixture was transferred to a Petri dish, dried at 100 °C for 6 h, and subsequently heated to 160 °C and kept for 6 h. The mixture was then transferred to a horizontal tubular furnace for carbonization at 900 °C for 2 h under $N_2$ flow with a heating rate of 60 °C $h^{-1}$. Excess amount of inorganic salt was removed by stirring the mixture in 1 M HCl for 3 d, followed by filtration and washing with large amounts of water. To reduce the content of oxygen-containing surface functionalities, the prepared carbon was treated under a reducing atmosphere (5% $H_2$ in $N_2$) in a horizontal tubular furnace for 2 h on 600 °C (heating rate: 240 °C $h^{-1}$).

*Synthesis of C/TAN*: Ball milling was performed using a Retsch PM 100 planetary ball mill, 12 mL stainless steel jars, and 5 stainless steel balls (10 mm diameter). Tannic acid (24 mg) and sustainable carbon (36 mg) were first neat ground for 50 min at 650 rpm. After the addition of propylene glycol (0.25 mL), the mixture was ground for an additional 10 min. Ethanol (0.75 mL) was added, and the mixture was ultrasonicated for 5 min, resulting in a homogeneous ink. Other grinding procedures were also tested as described in the results and discussion section. Electrodes were prepared by the addition of 40 µL ink on carbon paper (Spectracarb 2050A-0550, non-teflonized, 11 mm diameter) and drying at 80 °C under vacuum for 17 h. Alternatively, for the bulk material tests, the prepared ink was transferred to a Petri dish with the help of two times 1 mL ethanol and dried at 80 °C under vacuum for 17 h.

*Characterization of Bulk Materials*: Nitrogen physisorption measurements were performed using a Quantachrome Quadrasorb SI porosimeter. Samples were cooled down with liquid $N_2$ to 77 K upon activation of the carbon at 150 °C for 20 h under vacuum. Inductively coupled plasma optical emission spectrometry (ICP-OES) was conducted using a Horiba Ultra 2 instrument equipped with photomultiplier tube detection. Samples were dissolved in aqua regia and filtered before analysis. Elemental analysis was performed with a Vario MICRO cube CHNOS Elemental Analyzer (Elementar Analysensysteme GmbH, Langenselbold, Germany) in the CHNS mode. UV/Vis spectra were recorded using a 2 mm path length quartz cuvette and an AppliedPhotonics Chirascan qCD spectrometer. Details of sample preparations are explained in the Supporting Information. The morphology of electrode surfaces was investigated by scanning electron microscopy (SEM, Zeiss Leo Gemini 1550). For the investigation acceleration voltage of 3.00 kV was used. Powder XRD measurements were performed on a Bruker D8 diffractometer with Cu-K$\alpha$ ($\lambda = 0.154$ nm) X-ray source equipped with a scintillation counter-Scinti-Detector. Diffraction data were recorded in the $2\theta$ range between 3° and 70° with an angular resolution of 0.03°. Before plotting, the data were smoothened using Savitzky-Holay method with "10 points of window" and second polynomial order. STEM images were acquired using a double-Cs-corrected Jeol ARM200F, equipped with a cold field emission gun, an EDS detector, and a Gatan Quantum GIF energy-filter, which were utilized for the EDS and EELS measurements. For all investigations, the acceleration voltage was set to 80 kV.

*Electrochemical Measurements*: All electrochemical measurements were carried out using an MPG2 potentiostat/galvanostat (BioLogic Instruments). Swagelok type cells were used. Li metal (Sigma Aldrich) was used as an anode, the organic material served as a cathode, and 100 µL of 1.0 M $LiPF_6$ dissolved in 50:50 (v/v) ethylene carbonate/diethyl carbonate (EC/DEC) was used as an electrolyte (Sigma Aldrich). A porous PP Celgard membrane was used as a separator. EIS spectra were measured at open-circuit voltage from 10 mHz to 20 kHz. Series resistance ($R_s$) and charge transfer resistance ($R_{ct}$) were evaluated based on the Nyquist plot. Error bars indicate the standard deviation of every experiment.

## Supporting Information

Supporting Information is available from the Wiley Online Library or from the author.

## Acknowledgements

The authors acknowledge help in the laboratory by Jessica Brandt and thank her for ICP-OES measurements. The authors furthermore thank Rona Pitschke for SEM measurements and Antje Völkel for help with elemental analysis. The authors appreciate financial support by the German Research Foundation (DFG, grant: LI 2526/4-1), German Federal Ministry of Education and Research [BMBF, grant number 13XP5050A], the Fraunhofer-Max Planck cooperation project [Glyco3Display] the Max Planck Society, and the Max Planck Institute of Colloids and Interfaces.

Open access funding enabled and organized by Projekt DEAL.

## Conflict of Interest

The authors declare no conflict of interest.

## Keywords

biomass, electrochemistry, energy storage, redox chemistry, sustainability, tannic acid

Received: September 2, 2020
Revised: November 9, 2020
Published online: November 18, 2020

[1] M. Armand, J.-M. Tarascon, *Nature* **2008**, *451*, 652.
[2] R. Marom, S. F. Amalraj, N. Leifer, D. Jacob, D. Aurbach, *J. Mater. Chem.* **2011**, *21*, 9938.
[3] J.-M. Tarascon, M. Armand, *Nature* **2001**, *414*, 359.
[4] M. S. Whittingham, *Chem. Rev.* **2004**, *104*, 4271.
[5] Y. Liang, Z. Tao, J. Chen, *Adv. Energy Mater.* **2012**, *2*, 742.
[6] T. B. Schon, B. T. McAllister, P. F. Li, D. S. Seferos, *Chem. Soc. Rev.* **2016**, *45*, 6345.
[7] S. Lee, G. Kwon, K. Ku, K. Yoon, S. K. Jung, H. D. Lim, K. Kang, *Adv. Mater.* **2018**, *30*, 1704682.
[8] G. Yang, Y. Zhang, Y. Huang, M. I. Shakir, Y. Xu, *Phys. Chem. Chem. Phys.* **2016**, *18*, 31361.
[9] J. Xie, Q. Zhang, *J. Mater. Chem. A* **2016**, *4*, 7091.
[10] S. Muench, A. Wild, C. Friebe, B. Häupler, T. Janoschka, U. S. Schubert, *Chem. Rev.* **2016**, *116*, 9438.
[11] Y. Wu, R. Zeng, J. Nan, D. Shu, Y. Qiu, S. L. Chou, *Adv. Energy Mater.* **2017**, *7*, 1700278.
[12] G. Milczarek, O. Inganas, *Science* **2012**, *335*, 1468.
[13] S. K. Kim, Y. K. Kim, H. Lee, S. B. Lee, H. S. Park, *ChemSusChem* **2014**, *7*, 1094.

[14] F. N. Ajjan, M. J. Jafari, T. Rębiś, T. Ederth, O. Inganäs, *J. Mater. Chem. A* **2015**, *3*, 12927.
[15] I. K. Ilic, M. Perovic, C. Liedel, *ChemSusChem* **2020**, *13*, 1856.
[16] F. Melone, R. Saladino, H. Lange, C. Crestini, *J. Agric. Food Chem.* **2013**, *61*, 9307.
[17] J. Y. Oh, Y. Jung, Y. S. Cho, J. Choi, J. H. Youk, N. Fechler, S. J. Yang, C. R. Park, *ChemSusChem* **2017**, *10*, 1675.
[18] A. Mukhopadhyay, Y. Jiao, R. Katahira, P. N. Ciesielski, M. Himmel, H. Zhu, *Nano Lett.* **2017**, *17*, 7897.
[19] P. L. de Hoyos-Martínez, J. Merle, J. Labidi, F. C. E. Bouhtoury, *J. Cleaner Prod.* **2019**, *206*, 1138.
[20] M. Y. Jia, L. S. Xu, Y. Li, C. L. Yao, X. J. Jin, *New J. Chem.* **2018**, *42*, 14576.
[21] Y. A. Lee, J. Lee, D. W. Kim, C. Y. Yoo, S. H. Park, J. J. Yoo, S. Kim, B. Kim, W. K. Cho, H. Yoon, *J. Mater. Chem. A* **2017**, *5*, 25368.
[22] K. Nakahara, J. Iriyama, S. Iwasa, M. Suguro, M. Satoh, E. J. Cairns, *J. Power Sources* **2007**, *165*, 870.
[23] I. Y. Jeon, Y. R. Shin, G. J. Sohn, H. J. Choi, S. Y. Bae, J. Mahmood, S. M. Jung, J. M. Seo, M. J. Kim, D. W. Chang, L. Dai, J. B. Baek, *Proc. Natl. Acad. Sci. USA* **2012**, *109*, 5588.
[24] J. Xu, J. Shui, J. Wang, M. Wang, H. K. Liu, S. X. Dou, I. Y. Jeon, J. M. Seo, J. B. Baek, L. Dai, *ACS Nano* **2014**, *8*, 10920.
[25] M. Vujković, L. Matović, J. Krstić, M. Stojmenović, A. Đukić, B. Babić, S. Mentus, *Electrochim. Acta* **2017**, *245*, 796.
[26] D. Leistenschneider, K. Zürbes, C. Schneidermann, S. Grätz, S. Oswald, K. Wegner, B. Klemmed, L. Giebeler, A. Eychmüller, L. Borchardt, *Carbon* **2018**, *4*, 14.
[27] H. Zhou, Y. Zhou, J. Xu, L. Liu, J. Ma, W. Zhang, K. Li, H. Zhang, K. Li, *ACS Sustainable Chem. Eng.* **2019**, *7*, 18534.
[28] S. Mardix, E. Alexander, O. Brafman, I. T. Steinberger, *Acta Crystallogr.* **1967**, *22*, 808.
[29] G. Štefanić, S. Krehula, I. Štefanić, *Chem. Commun.* **2013**, *49*, 9245.
[30] T. B. Schon, A. J. Tilley, C. R. Bridges, M. B. Miltenburg, D. S. Seferos, *Adv. Funct. Mater.* **2016**, *26*, 6896.
[31] I. K. Ilic, K. Leus, J. Schmidt, J. Hwang, M. Maranska, S. Eigler, C. Liedel, *ACS Sustainable Chem. Eng.* **2020**, *8*, 3055.
[32] N. Patil, A. Aqil, F. Ouhib, S. Admassie, O. Inganäs, C. Jérôme, C. Detrembleur, *Adv. Mater.* **2017**, *29*, 1703373.
[33] R. Yan, M. Antonietti, M. Oschatz, *Adv. Energy Mater.* **2018**, *8*, 1800026.